Available online at www.sciencedirect.com

SciVerse ScienceDirect

Ceramics International 39 (2013) 7355–7365

CERAMICS INTERNATIONAL

www.elsevier.com/locate/ceramint

Substrate heating and post-annealing effect on tungsten/tungsten carbide bilayers grown by non-reactive DC magnetron sputtering

L.C. Agudelo-Morimitsu[a,b], J. De La Roche[a,b], D. Escobar[a,b], R. Ospina[a], E. Restrepo-Parra[a,b,*]

[a]*Laboratorio de Física del Plasma, Universidad Nacional de Colombia, Sede Manizales, Km. 9 vía al aeropuerto, Campus La Nubia, Manizales, Colombia*

[b]*PCM Computational Applications, Universidad Nacional de Colombia, Sede Manizales, Km. 9 vía al aeropuerto, Campus La Nubia, Manizales, Colombia*

Received 7 November 2012; received in revised form 22 February 2013; accepted 22 February 2013
Available online 14 March 2013

Abstract

Tungsten–tungsten carbide (W/WC) bilayers were produced by non-reactive DC magnetron sputtering at various substrate temperatures between room temperature and 300 °C. The coatings were characterized in terms of morphology, structure and chemical composition using several techniques such as X-ray diffraction (XRD), Raman Spectroscopy, Auger Electron Spectroscopy (AES), Scanning Electron Microscopy (SEM), Energy Dispersive Spectroscopy (EDS) and Scanning Probe Microscopy (SPM) in the Atomic Force Microscopy (AFM) mode. Bragg peaks corresponding to the (110) diffraction plane of the W phase and (111), (200), (220) and (311) peaks corresponding to the cubic WC phase were identified. From the XRD analysis, a strong influence of the substrate temperature on the grain size and crystallographic texture was observed; nevertheless, a poor influence on the lattice parameter and microstrain was detected. Furthermore, different vibrational modes of the W–C structure and characteristic peaks corresponding to O–W–O bonds were observed. Depth profile analysis was also carried out using AES, which revealed the presence of C, W, O and Fe. Initially, carbon and tungsten were observed in the WC layers. After the films were totally etched, Fe from the substrate was detected. However, the morphology was not significantly affected by temperature. An important result was the improvement in the coatings' adherence when an interlayer of W was inserted. In this work, the bilayers' behavior during annealing was also studied. The films were observed to oxidize at approximately 600 °C.

Keywords: XRD; Raman; AES; SEM; AFM

1. Introduction

Transition metal carbide thin films present excellent properties such as high hardness, low wear and chemical and thermal stability. Thus, they are frequently used in cutting tools, thermal barriers and microelectronic devices [1–3]. Tungsten carbide (WC) thin films exhibit a favorable combination of hardness, above 18 GPa, a low wear coefficient and a high corrosion resistance and oxidation temperature [4–7]. These properties are very useful in the metallurgical industry and in developing thermal barriers for nuclear reactors [7]; moreover, recent studies have reported the incorporation of this material in fuel cell cathodes and in electrocatalysts for alkane reforming and isomerization [8]. The W–C phase diagram describes three different carbide structures: a cubic carbide WC_{1-x} phase for $0.34 \leq x \leq 0.43$ with a NaCl structure, hexagonal stoichiometric monocarbide WC and second hexagonal carbide W_2C. The WC_{1-x} and W_2C phases are stable between 1250 and 2500 °C, and hexagonal monocarbide WC is the only thermodynamically stable phase at room temperature [2,9]. Nevertheless, the formation and stability of WC phases may depend on fabrication conditions;

*Corresponding author at: Laboratorio de Física del Plasma, Universidad Nacional de Colombia, Sede Manizales, Km. 9 vía al aeropuerto, Campus La Nubia, Manizales, Colombia. Tel./fax: +57 6 8879495.
E-mail address: erestrepopa@unal.edu.co (E. Restrepo-Parra).

0272-8842/$ - see front matter © 2013 Elsevier Ltd and Techna Group S.r.l. All rights reserved.
http://dx.doi.org/10.1016/j.ceramint.2013.02.075

therefore, many authors have focused on the synthesis process of WC films using several physical vapor deposition (PVD) and chemical vapor deposition (CVD) techniques [5], thereby obtaining certain WC phases or combinations thereof. However, to improve some of the physical properties of this material, it has been deposited as bilayers and multilayers [6,8]. It is well known that one of the most challenging issues associated with such protective coatings is their adhesion to substrates [10–12]. Normally their adhesion is strongly affected by residual stress. The high residual stress generated in hard coatings during the deposition process easily results in the detachment of the coatings from substrates and limits their practical use in applications that require superior hardness [13]. Sometimes, the residual stress in hard coatings can take on values on the order of 4 GPa [14]. Several methods have been extensively used to improve the adhesion between these coatings and substrates, such as ion bombardment prior to deposition [15], the insertion of a metal interlayer between the films and their substrates [16] and coating in multilayers or compositional gradients [17]. The insertion of a metallic interlayer is normally used to relax the residual stress generated at the coating–substrate interface.

The physical properties of thin films are often anisotropic and are normally controlled by their specific microstructure, including the atomic ratio (stoichiometry) of their components, crystallinity and preferred orientation, which are complex functions of the deposition parameters of a given growth method [18,19]. The substrate temperature has a strong influence on films' structural and morphological characteristics because these properties are correlated with the thermal energy used to condense the material on a substrate surface [20]. For instance, in their study on W/WC coatings produced by pulsed vacuum arc discharge. Ospina et al. [21] observed a structural and morphologic evolution in the films.

This paper presents a study on W/WC bilayers deposited on stainless steel substrates (316L) by a DC magnetron sputtering technique at various substrate temperatures. The effect of deposition temperature on the microstructure and morphological and chemical composition of the resulting coatings was analyzed. Moreover, the effect of interlayer insertion on the films' adherence was studied. A post-annealing process was also applied to study the oxidation of coatings.

2. Experimental setup

Tungsten and tungsten carbide (W/WC) bilayers were deposited by a DC magnetron sputtering technique using tungsten (6 N) and 50/50 tungsten carbide (6 N) targets measuring 5 cm in diameter for the W and WC layers, respectively. The coatings where grown on 316L stainless steel substrates at various substrate temperatures (T_S) between room temperature (RT) and 300 °C. The substrates were ultrasonically cleaned in acetone for 15 min. They were held under a vacuum pressure of 10^{-4} Pa and plasma cleaned for 15 min prior to deposition. The bilayer deposition conditions were as follows: an operating pressure of 6 Pa, a power density of 5 W cm^{-2}, an Ar gas flow rate of 20 sccm and a deposition time of 60 min.

Structural characterization was performed with a Bruker AXS D8 advance X-ray diffractometer (XRD), using grazing incidence with Cu-k$_\alpha$ radiation (λ=1.5406 Å) between 30° and 80°, with increments of 0.02 made every 2 s. Auger electron spectroscopy (AES) was used to probe the compositional chemical gradient of the deposited films. An electron beam of 3 keV was used. The analysis was carried out using 10 scans for each element, with steps of 0.5 eV and a step time of 50 ms. Depth profiles were obtained using an Ar^+ ion beam with an energy of 5.0 keV and current density of 30 μA/cm^2 at a pressure on the order of 6×10^{-6} Pa. Raman measurements between 200 cm^{-1} and 1600 cm^{-1} were carried out with a LabRam Horiba Yvon spectrometer featuring hole and slit widths of 1000 μm, using the 473 nm line of a 20 mW DPSS laser. For morphologic characterization (grain size), scanning probe microscopy (SPM) in the atomic force microscopy (AFM) mode was used. For this study, a Park Scientific Instruments Autoprobe CP with silicon probes and ProScan image processing software were used. To obtain topographic images of the films, AFM mode was employed, using a silicon nitride (Si_3N_4) cantilever probe with a spring constant of 0.16 N/m, a scanning speed of 1 Hz and an image resolution of 256 × 256 pixels. Measurements were carried out in 60% relativity humidity at 24 °C (room temperature). The results were obtained by averaging five measurements taken at different points of each coating. Energy dispersive spectroscopy (EDS) analyses was carried out using a Philips XL-30TMP scanning electron microscope (SEM) with a standard EDAX probe at an energy of 20 keV and a magnification of 200×. Thickness and roughness measurements were also performed with an Ambios Technologies XP2 profilometer, using a distance of 0.4 mm and a range of 10 μm for measuring roughness.

3. Results and discussion

3.1. X-ray diffraction

Fig. 1 shows the diffraction patterns of W/WC bilayers deposited at T_S from RT to 300 °C on 316L stainless steel substrates. Bragg peaks corresponding to the (110) diffraction plane of W phase at 36.9° and peaks of the (111), (200), (220) and (311) planes corresponding to the cubic WC phase are presented [22]. The intensity, broadening and shape of the peaks vary as a function of T_S. To study the evolution of W/WC bilayers' microstructure, the lattice parameter, crystallite size, microstrain and crystallographic texture were analyzed.

Fig. 2(a) shows the variation in the lattice parameter as a function of T_S. No evident influence of T_S on this

parameter was observed, and the values were lower than those reported in the literature for WC. The lattice parameter calculated by FCC–WC phase simulation has been reported to be $a=4.39$ Å [8], while experimental values between 4.22 and 4.27 Å have been reported [9,23]. It is well known that the lattice parameter is highly influenced by the stress in films. A decrease in the lattice parameter indicates compressive stress [24]. To calculate the crystallite size and microstrain, the double-Voigt method was used, assuming a Voigtian (i.e., pseudo-Voigt) profile for the experimental peaks.

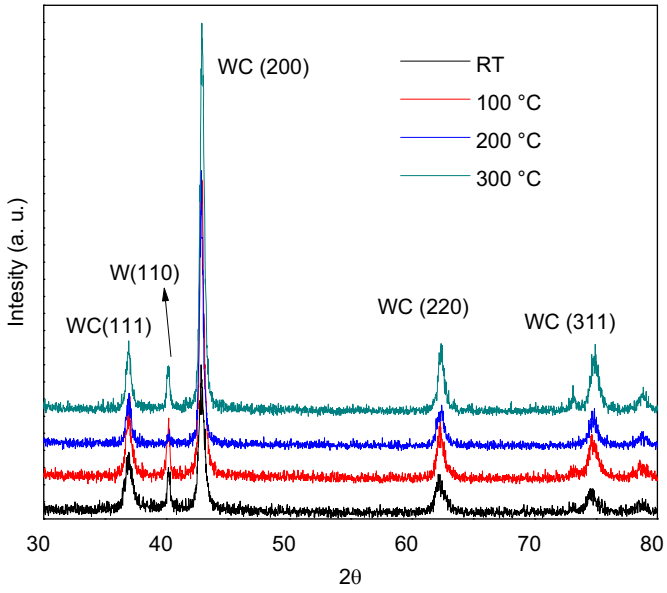

Fig. 1. X-ray diffraction patterns for W/WC bilayers deposited by magnetron sputtering on stainless steel 316L at different substrate temperatures (T_S).

Fig. 2(b) shows the variation in crystallite size as a function of T_S. In general, the crystallite size increases as the adatom mobility and surface diffusion increase, favoring nucleation and coalescence. This leads to a reduction in the number of nucleation points [25–27]. An increase in domain size implies a reduction in the number of domain boundaries affecting lattice distortion and hence the microstrain [28,29]. Domain boundaries represent sources of high deformation in crystalline materials; thus, a decrease in the number of domain boundaries involves a diminution in the average microstrain, as shown in Fig. 2(c). In the case of $T_S=100$ °C, this temperature represents a crystal relaxation, showing a high reduction of microstrain without affecting a number of domain boundaries.

Texture analysis was also carried out, and the results of this analysis for several reflections as a function of T_S are shown in Fig. 2(d). An increment in the texture coefficient

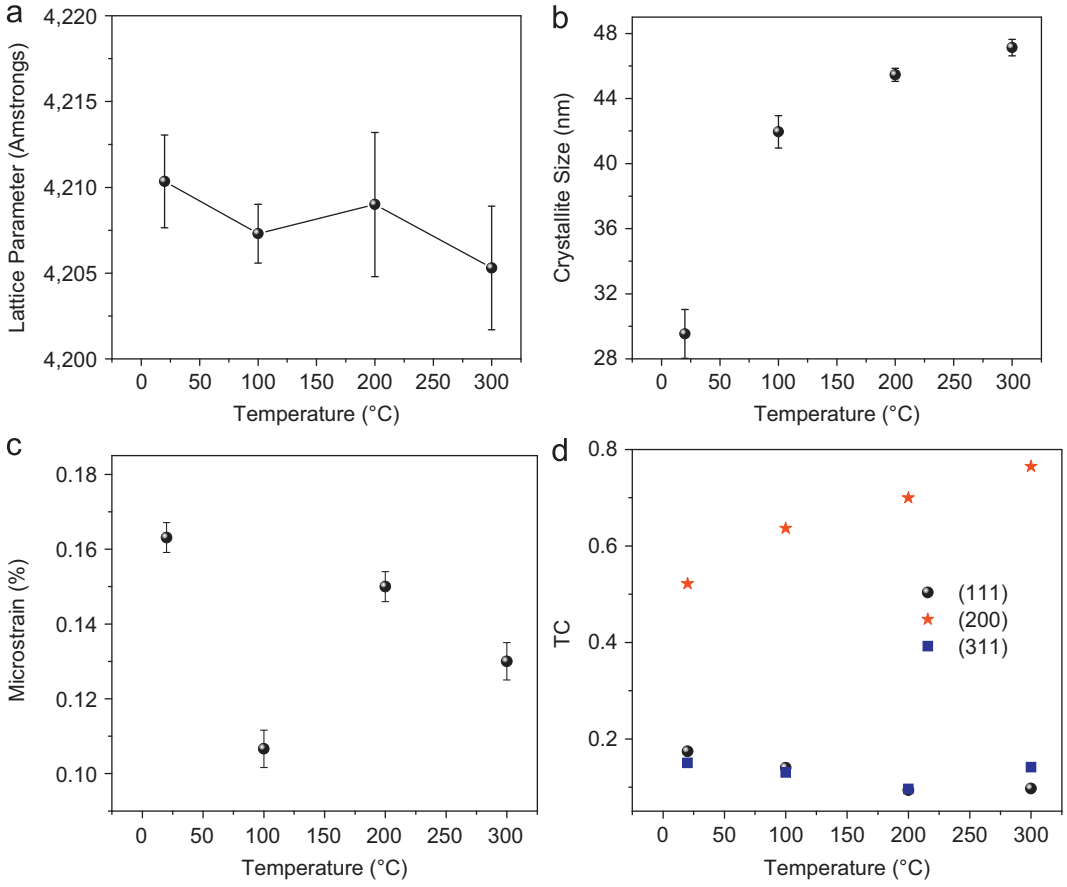

Fig. 2. Data obtained by XRD as a function of T_S: (a) lattice parameter, (b) crystallite size, (c) microstrain average and (d) crystallographic texture.

(TC) in the case of the (200) crystallographic orientation can be observed, while there is a slight reduction in TC along the (111) and (311) orientation planes. In general, the peak intensity of the (200) planes is greater than that of others, including the (111) plane. This result has been reported in several works carried out by Larsson et al. [30]. The fact, that the preferred orientation is favored for the (200) direction rather than (111) can be explained by taking into account studies carried out by Bruneaux et al. [31] and later confirmed by Oh and Je [32] and Oh et al. [33]. The model developed by these researchers was used to explain changes in the preferred orientation commonly observed with variations in layer thickness. These studies suggest that he preferred orientation is determined by the competition between two thermodynamic parameters, free energy and deformation energy. It was established that, for thicknesses below a certain critical value, layers present a preferred orientation corresponding to low surface energy. This argument is based on a large number of broken bonds along certain planes. As the layer thickness increases, the deformation energy increases, while the surface energy is not significantly affected. As will be discussed later, the thickness increases only slightly as a function of T_S [29]. It is assumed that the deformation state is a consequence of elastic deformations produced when new crystals are accommodated into sites occupied by other previously formed crystals. It is also due to the compressive residual stress generated during the deposition process, caused by highly energetic particles that hit the surface with large momentum, at high voltages and low working pressures [34–36]. T_S variations during the deposition process influence the evolution of texture: at low T_S, the mobility of surface adatoms is low and hence so is the texture. Even for thick layers, the texture is determined during the initial stages of deposition, when nucleation is highly important. According to Thompson et al. [37], the (111) orientation, which exhibits greater atomic packing, is not favored (decreases) with increasing temperature; thus, the mobility of adatoms increases. As T_S increases, there is greater adatom relaxation and accommodation, decreasing the deformation energy associated with this specific orientation. Considering that the surface energy is associated with the (200) direction, not only can an increase in energy as a function of T_S be assumed but there is also greater mobility in the grain boundaries because the growth process is dominated by surface energy.

To study the evolution of W/WC bilayers submitted to a post-annealing treatment in air at atmospheric pressure, diffraction patterns at high temperatures were obtained for the sample grown at 300 °C due to the good microstructural features of this sample. Fig. 3 shows the diffraction patterns obtained for the as-deposited W/WC bilayer heated at annealing temperatures (T_a) of 200, 400 and 600 °C. At T_a=400 °C, the W and WC phases remained almost unaffected. Nevertheless, at 600 °C, oxidation (WO_3) and a decrease in the WC peak intensities can be observed, indicating the degradation of coating. According

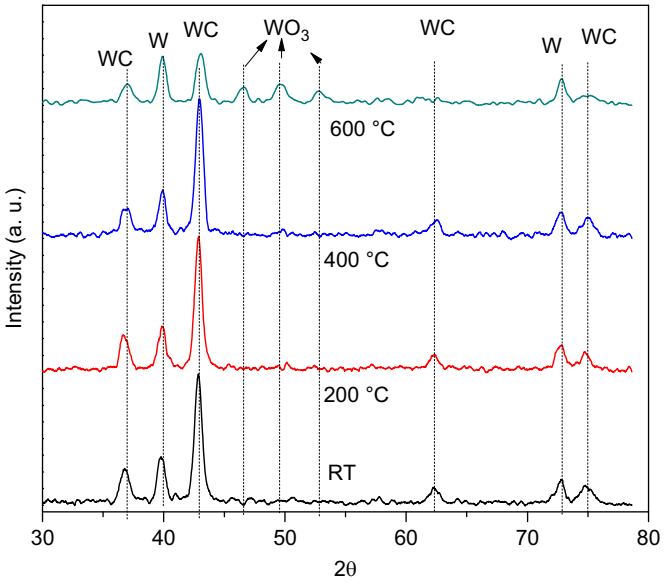

Fig. 3. Diffraction patterns obtained for W/WC sample grown at T_S=300 °C and treated with an annealing process at 200, 400 and 600 °C.

to the results, the W layer is unaffected by the oxidation process because it does not have direct contact with the environment, while the WC layer undergoes strong changes. Oxygen in the environment reacts with the coating at temperatures between 400 and 600 °C. According to thermodynamics, it can be deduced that carbon is oxidized to form volatile compounds, while W forms oxides that remain on the surface [38].

3.2. Raman Spectroscopy

Fig. 4(a) presents Raman spectra for W/WC bilayers grown on 316L stainless steel obtained at different T_S. In this figure, different vibrational modes of the W–C structure and characteristic peaks belonging to the bending modes of O–W–O bonds at bands approximately 400 cm^{-1} are identified [39]. Although no oxide phases were revealed by the XRD analysis, they may occur as an amorphous phase. However, the characteristic D and G bands of C bonds were not detected. This implies that the highest quantity amount of carbon must be present in W–C bonds belonging to part of the cubic structure, as previously observed by the XRD analyses [40]. Moreover, the presence of D and G bands in WC coatings is typical when these materials are synthesized using hydrocarbides as precursors (methane, acetylene, etc). For instance, Radic et al. [41] synthesized nanocrystalline WC by reactive DC magnetron sputtering with a gas mixture of Ar and C_6H_6 and a tungsten target, varying the C_6H_6 percentage. As this percentage decreased, a reduction in the Raman peak intensities corresponding to the D and G bands of carbon was observed, and at low concentrations of gas, these bands practically disappeared. In this study, coatings were produced using a non-reactive process (only

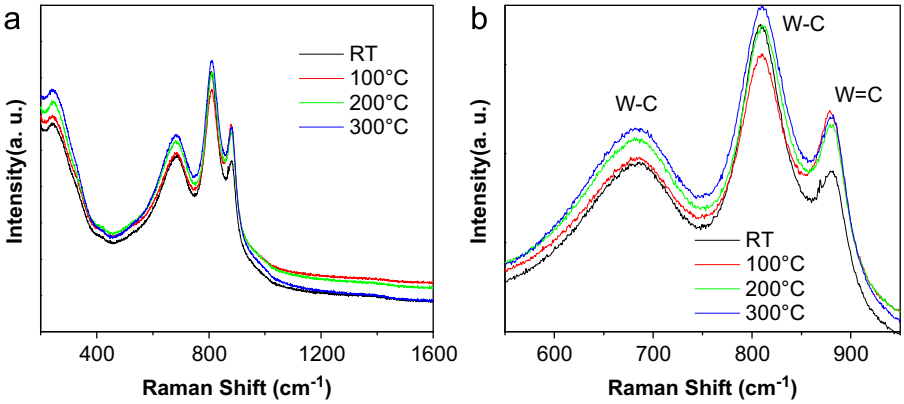

Fig. 4. (a) Raman spectra of W/WC bilayers obtained at different T_S on stainless steel 316L and (b) peaks associated with bands WC.

Ar was used as the working gas) and a WC target; consequently, these bands were not formed. However, bands located approximately between 700 and 800 cm^{-1} can be associated with stretching modes of W–C [42]. According to the analysis carried out by Yang et al. [42], small band shifts at temperatures between 400 and 800 °C can be related to changes in crystalline phases and also to the amount of carbon in a sample. The coatings fabricated in our study were produced at a T_S below 300 °C; thus, peak shifts can be neglected. The increase in the peak intensities as a function of T_S may be due to the increase in the number of bonds corresponding to WC. This result is in agreement with the experimental data obtained from the XRD analyses that show an increment in the diffraction peak intensities as a function of T_S. In addition, according to the results regarding film thickness, which will be discussed later, the thickness increases as a function of T_S, generating a greater number of crystallographic planes. In Fig. 4(b), three peaks associated with WC bands at approximately 681.5, 809.2 and 880.9 are observed. According to previous reports, the two first bands correspond to the stretching mode of W–C [43] and the last one could be associated with the stretching mode of W=C bonds. The increase in band broadening with T_S may be due to the existence of a certain distortion in the lattice of the crystalline structure, which could lead to a phase transformation from FCC to HCP if T_S continues to increase [44,45].

3.3. Auger Electron Spectroscopy (AES)

The AES spectra in Fig. 5 show the elemental composition of the W layer and W/WC bilayer of the coatings grown on 316L stainless steel at 300 °C. The atomic percentage deduced from the surface and depth profiles is presented in Fig. 5(a). The characteristic elements of the studied materials and oxygen in the W layer are observed; however, oxygen practically disappears in the W/WC bilayer. This is because metals tend to form surface oxide layers as a protection against corrosion [44]. The presence of oxygen can also be attributed to sample contamination that may have occurred when the sample was exposed to the environment after deposition. The depth profile in Fig. 5(b) shows the atomic concentration as a function of depth during etching. The depth profile also shows the presence of C, W, O and Fe. Initially, carbon and tungsten from the WC layers were observed. From this profile, the WC composition can be calculated quantitatively because the thickness is greater than the resolution limit of the equipment. As shown in Fig. 5(b), the W/C ratio is on the order of 0.55/0.27–2. Neglecting contributions due to oxygen and preferential sputtering effects, the WC_x stoichiometry can be determined, where $x \sim 0.27$. This result was confirmed by EDS measurements, which indicated a carbon content of approximately 26.85%. This type of stoichiometric analysis has been reported by Gubisch et al. [46]. The literature reports stoichiometry values (x) similar to those obtained in this work [47–49]. From the depth profile, the layer thickness can be estimated. Assuming an erosion rate on the order of 2 nm/min, the bilayer elements disappear after approximately 415 min, revealing the presence of Fe, the layer thickness of which is approximately 830 nm. This value is similar to that obtained from SEM and profilometry analyses, which will be discussed later. It can be concluded that the thicknesses of the W and WC layers are approximately 360 nm and 470 nm, respectively.

3.4. Scanning Electron Microscopy

Fig. 6(a) shows an SEM image of a WC film grown on 316L stainless steel at 300 °C without a W layer, this figure shows delamination occurring in the film. To improve film adhesion, a buffer layer is normally employed in PVD processes [50] (see Fig. 6(b)) because films are affected by the stress generated by a lack of chemical synergy, crystalline structure coupling, lattice parameter mismatch and differences in thermal expansion coefficients.

In general, the type of interface formed between a substrate and coating will dominate the adhesion behavior [51]. In the case of nitride and carbide coatings deposited on steel, metallic interfaces are often used to prevent

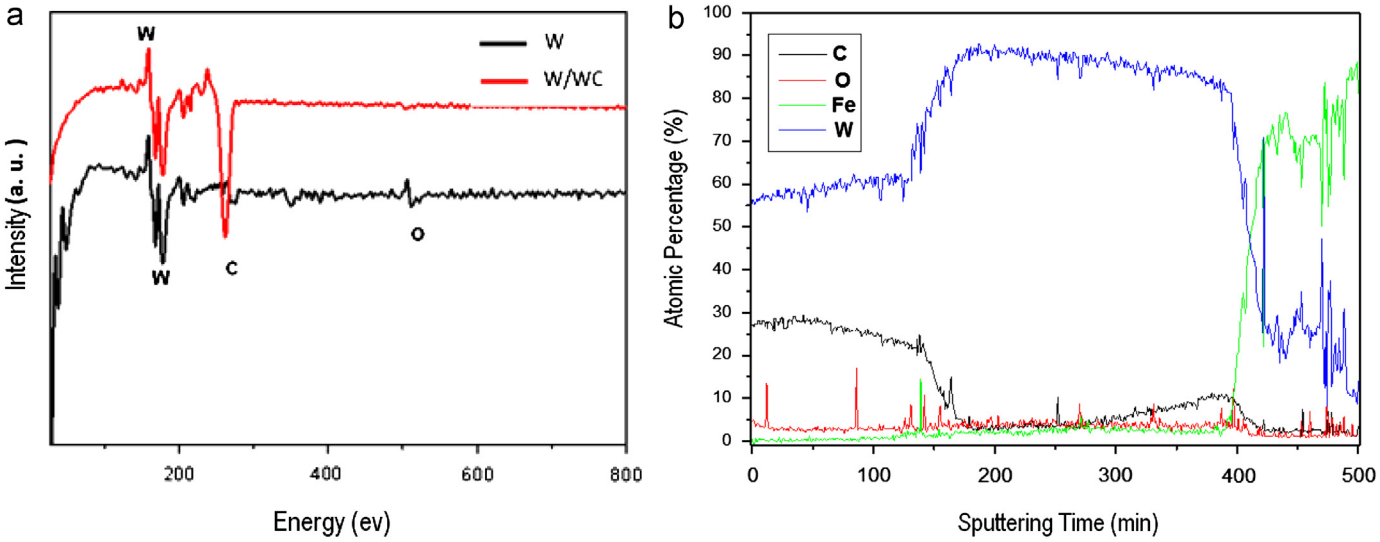

Fig. 5. (a) Auger electron spectra obtained for W and WC bilayers and (b) depth profile of W/WC bilayer grown at T_S=300 °C.

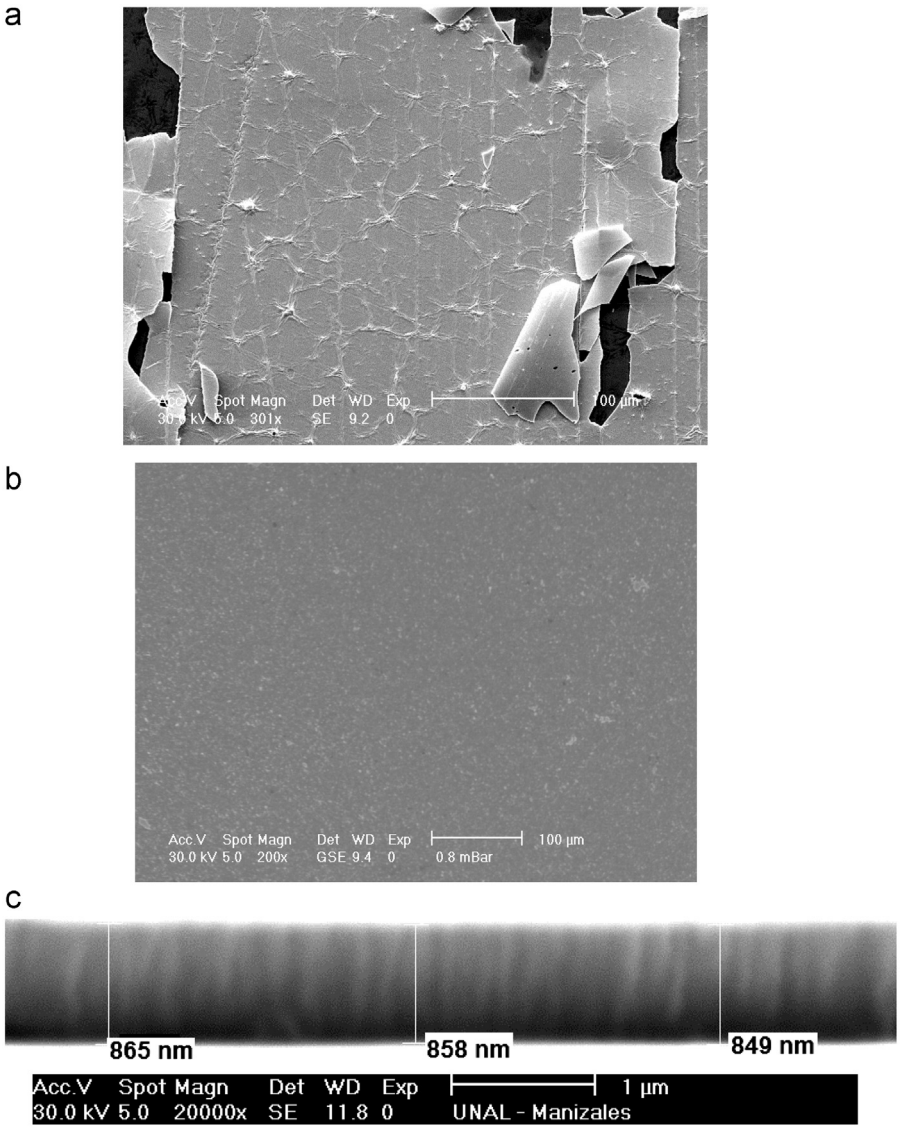

Fig. 6. SEM micrographs of (a) WC deposited on stainless steel 316L at T_S=300 °C, (b) W/WC coating grown at T_S=300 °C and (c) cross section W/WC bilayer grown on stainless steel 316L at T_S=300 °C.

graphitization, increasing chemical affinity and stabilizing carbon–carbon bonds [52]. The functions of interfaces generally include (i) improving the nucleation rate of the ceramic layer [53,54], (ii) improving adhesion forces, (iii) minimizing residual thermal stress [55], (iv) improving the barriers to carbon diffusion to maintained a constant concentration of carbon during nucleation and growth processes [56] and (v) increasing structural compatibility for the nucleation of WC crystals. In this study, the W interface significantly improved the adherence of W/WC coatings. The SEM in Fig. 6(c) shows the thickness of the W/WC coating obtained at 300 °C. The thickness is approximately 850 nm, similar to that obtained by depth profile analysis. This image shows the columnar growth of the bilayer, as reported in the literature for materials grown by using PVD techniques [29].

3.5. Energy Dispersive X-ray Spectroscopy (EDS)

Using EDS, the characteristic M and L peaks of W, with energy values of 1.779 eV and 8.395 eV, respectively, were observed. In addition, peaks corresponding to 316L stainless steel substrate were identified. These peaks could be observed because the penetration depth of the electron beam was greater than the film thickness. EDS spectra obtained for the WC layer reveal peaks corresponding to W and C. Table 1 shows the concentration of all elements presented in EDS spectra.

The dependence of W and C atomic percentages on T_S for W/WC samples grown on 316L stainless steel substrates was determined. These values are shown in Table 1. In all cases, the amount of tungsten is greater than that of carbon. From the phase diagram [57], it can be concluded that the WC stable phase is produced over a small range of concentrations; therefore, the amount of carbon must be controlled to obtain this specific WC phase [58]. These results are in agreement with AES depth profile measurements. The increase in T_S facilitates the formation W–C bonds and an increment in the carbon percentage is observed. This can lead to the stoichiometric formation of the hexagonal WC phase, according to the literature [42]. It is necessary to take into account the fact that EDS spectra include the contributions of both the WC and W layers, leading to a higher W peak intensity. Upon increasing the temperature, the WC layer thickness tends to increase, as will be discussed later. This effect decreases the effect of W layer on EDS emission that contributes strongly to the total intensity of the tungsten peak.

Table 1
Atomic percentages (at%) of W and WC monolayers and W/WC bilayers determined by EDS.

	C	W	O	–
Monolayers				
W	–	35.24 ± 0.35	31.46 ± 2.5	–
WC	21.81 ± 1.1	70.01 ± 0.68	8.14 ± 0.78	–
Temperature (°C)	**C**	**W**	**O**	**W/C**
W/WC bilayers				
RT	21.22 ± 0.5	59.09 ± 0.2	5.56 ± 0.3	2.66
100	23.26 ± 0.3	58.60 ± 0.3	5.00 ± 0.4	2.52
200	23.39 ± 0.4	58.28 ± 0.2	5.50 ± 0.2	2.49
300	26.85 ± 0.3	55.53 ± 0.2	4.63 ± 0.4	2.06

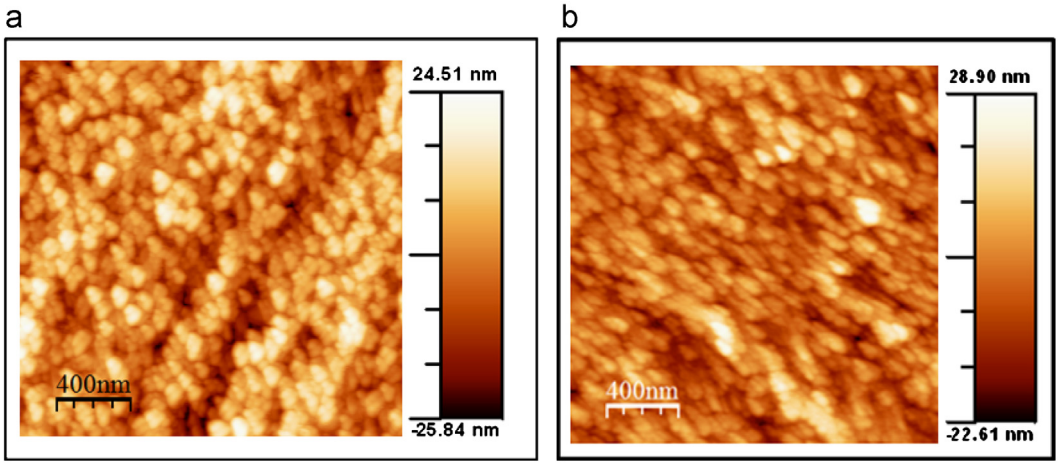

Fig. 7. AFM images of (a) W and (b) WC monolayers.

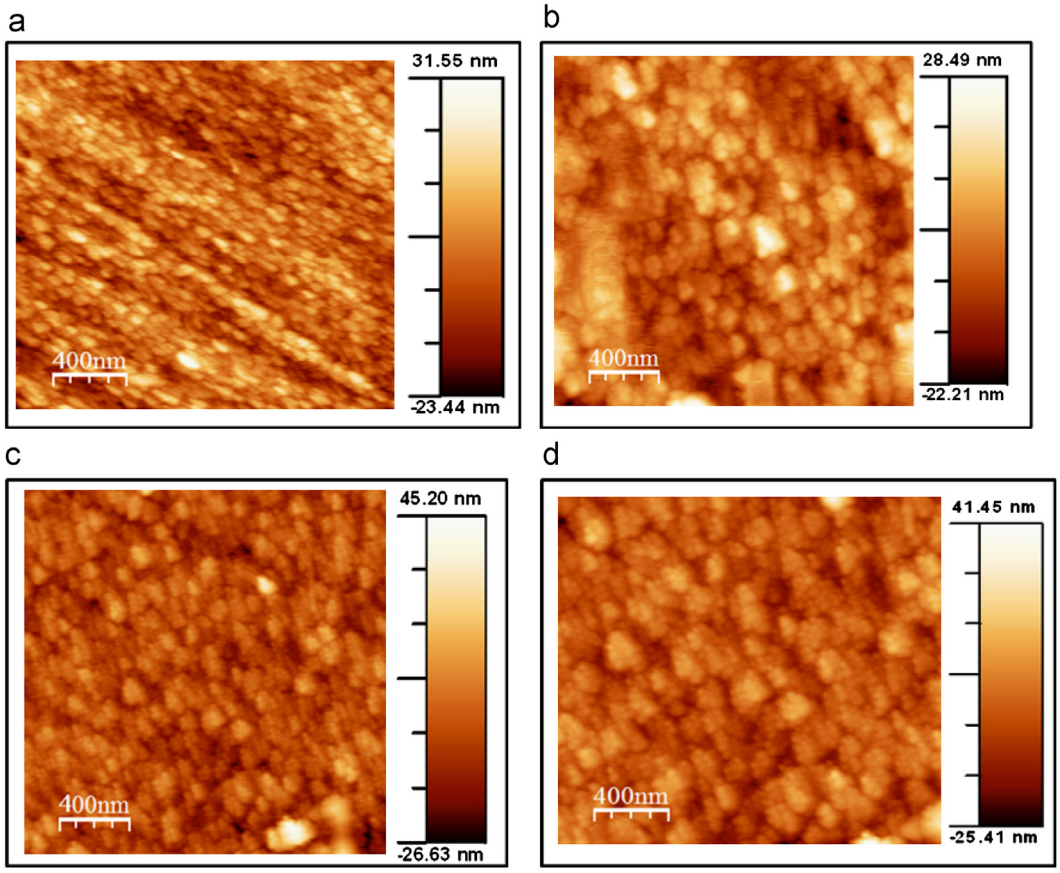

Fig. 8. AFM images of (a) W/WC bilayer grown at RT, (b) W/WC bilayer grown at 100 °C, (c) W/WC bilayer grown at 200 °C and (d) W/WC bilayer grown at 300 °C on stainless steel 316L.

Table 2
Roughness, grain size and thickness determined by atomic force microscopy analysis of monolayers and W/WC coatings grown on stainless steel 316L at different T_S.

Material	Roughness (nm)	Grain size (nm)	Thickness (nm)
Monolayers			
316L	54.67 ± 2.1	–	–
W	8.07 ± 0.2	90.66 ± 0.3	780.34 ± 10.3
WC	6.98 ± 0.3	92.78 ± 0.5	730.04 ± 12.4
Temperature (°C)			
W/WC bilayers			
RT	7.02 ± 0.05	112.67 ± 0.04	834.00 ± 10.3
100	6.86 ± 0.03	110.73 ± 0.05	850.33 ± 10.1
200	6.85 ± 0.04	108.68 ± 0.03	876.33 ± 5.32
300	6.84 ± 0.03	98.33 ± 0.02	846.67 ± 11.3

3.6. Atomic Force Microscopy (AFM)

AFM analysis allowed for the morphology of the coating surfaces to be studied and the grain size obtained. Fig. 7(a,b) presents AFM images of W and WC monolayers grown at T_S=300 °C on 316L stainless steel. In these images, a morphology typical of this type of coating can be observed, presenting a grain size on the order of few nanometers.

Fig. 8(a–d) shows AFM images of W/WC bilayers grown at different T_S. The grain size is shown in Table 2. A slight diminution in grain size can be observed. This reduction can be explained by employing the qualitative model proposed by Movchan and Demchishinh and later modified by Martin et al. [59]. During film synthesis, nucleation and subsequent formation of very small granular structures occur. When a layer is transformed into a continuum material, surface diffusion allows adatoms to

migrate between neighboring grains. In addition, crystals with lower surface energy incorporate more material, growing above neighboring crystals with higher surface energy. This competition leads to a decrease in grain size because larger grains contribute to the formation of new grains or to the growth of smaller grains [60].

3.7. Profilometry analyses

Table 2 presents the RMS roughness and thickness of the W, WC and W/WC bilayers as a function of T_S. In general, the roughness depends on several parameters, the most important of which is the energy of the plasma-generated species emanating from the target and striking the substrate surface, the substrate temperature and the coating composition [61].

The results show a slight tendency for the surface roughness to decrease with increasing substrate temperature. As T_S increases, the high thermal energy available in the substrate contributes to the formation of new, larger surface grains. Similar results have been observed in studies by Devika et al. [62], who reported a decrease in roughness with increasing T_S. In Table 2, the thickness also shows a slight increase as a function of T_S.

4. Conclusions

W and WC monolayers and W/WC bilayers were produced by DC magnetron sputtering at various substrate temperatures ranging from room temperature to 300 °C. The coatings were characterized in terms of composition, structure and morphology.

The XRD analysis revealed the presence of BCC phase of W and FCC phase of WC, presenting a greater lattice parameter than that reported for bulk materials, which is common in thin film growth. In addition, a preferred orientation along the (200) direction was observed; this effect was attributed to the small dimensions of the films, which lead to a greater surface energy compared with the deformation energy.

Chemical composition analysis was carried out by Raman and Auger spectroscopy techniques. The Raman spectra reveal the presence of W–O, W–C and W═C bonds. Additionally, there was no evidence of D and G bands corresponding to carbon. This may be because hydrocarbides were not used for layers grown growth. A depth profile analysis was carried out for W/WC bilayer grown on steel substrates (316L), and the presence of W and C was observed during the first few minutes of the sputtering process. The stoichiometric concentration of WC (~2) is similar to that indicated by EDS analysis. From the depth profile analysis, the coating thicknesses were also obtained and were similar to those obtained by profilometry.

Using EDS, the atomic percentages of the components of the bilayers were obtained. The results showed a lower concentration of carbon relative to that of tungsten, defining a non-stoichiometric phase. The carbon concentration was observed to increase with the substrate temperature, which could generate a slight increase in film thickness. Morphology studies were carried out on W/WC coatings grown at different substrate temperatures using AFM, SEM and profilometry techniques. As T_S increased, a slight decrease in roughness and grain size was observed, due to the competition between the forces affecting these two properties, also, to the high mobility of adatoms and the improvement in film packing. Profilometry revealed a slight increase in film thickness with T_S, due to increase in the carbon concentration and the bond formation W–C. SEM micrographs also indicated poor adherence of WC monolayers on 316L substrates. This adherence is considerably improved by the insertion of a W interlayer.

Acknowledgments

The authors gratefully acknowledge the financial support of "La Dirección Nacional de Investigaciones de la Universidad Nacional de Colombia, sede Manizales (DIMA)" during the course of this research under the projects "Producción y Caracterización de recubrimientos con aplicaciones industriales y biocompatibles" and "Síntesis y estudio del comportamiento de bicapas de tungsteno, carburo de tungsteno (W/WC) obtenidas por la técnica sputtering DC".

References

[1] H. Qu, S. Zhu, Q. Li, C. Ouyang, Influence of sintering temperature and holding time on the densification, phase transformation, microstructure and properties of hot pressing WC–40 vol% Al_2O_3 composites, Ceramics International 38 (2012) 1371–1380.
[2] K. Abdelouahdi, C. Sant, F. Miserque, P. Aubert, Y. Zheng, C. Legrand-Buscema, J. Perrière, Influence of CH(4) partial pressure on the microstructure of sputter-deposited tungsten carbide thin films, Journal of Physics: Condensed Matter 18 (2006) 1913–1925.
[3] T. Dash, B.B. Nayak, Preparation of WC–W_2C composites by arc plasma melting and their characterizations, Ceramics International, http://dx.doi.org/10.1016/j.ceramint.2012.10.016.
[4] G. Zambrano, P. Prieto, F. Perez, C. Rincon, H. Galindo, L. Cota-Araiza, J. Esteve, E. Martinez, Hardness and morphological characterization of tungsten carbide thin films, Surface and Coating Technology 108 (1998) 323–327.
[5] J.-P. Palmquist, Z. Czigany, M. Oden, J. Neidhart, L. Hultman, U. Jansson, Magnetron sputtered W–C films with C_{60} as carbon source, Thin Solid Films 444 (2003) 29–37.
[6] E. Harry, A. Rouzaud, P. Juliet, Y. Pauleau, General properties and scratch adhesion characterization of carbon-containing tungsten films, Surface and Coating Technology 116–119 (2009) 81–85.
[7] H. Zhang, D.Y. Li, Effects of sputtering condition on tribological properties of tungsten coatings, Wear 255 (2003) 924–932.
[8] M.A. Neto, E.L. Silva, A.J.S. Fernandes, F.J. Oliveira, R.F. Silva, Deposition of alpha-WC/a-C nanocomposite thin films by hot-filament CVD, Surface and Coating Technology 206 (2011) 103–106.
[9] E. Raekelboom, K. Abdelouahdi, C. Legrand-Buscema, Structural investigation by the Rietveld method of sputtered tungsten carbide thin films, Thin Solid Films 517 (2009) 1555–1558.
[10] P. Richard, J. Thomas, D. Landolt, G. Gremaud, Combination of scratch-test and acoustic microscopy imaging for the study of coating adhesion, Surface and Coating Technology 91 (1997) 83.

[11] T. Nsongo, M. Gillett, Adhesion characterization of titanium and titanium nitride thin coatings on metals using the scratch test, Journal of Adhesion and Adhesives 15 (1995) 191.
[12] Y.S. Hong, S.H. Kwon, T. Wang, D.-I. Kim, J. Choi, K.H. Kim, Effects of Cr interlayer on mechanical and tribological properties of Cr–Al–Si–N nanocomposite coating, Transactions of Nonferrous Metals Society of China 21 (2011) s62–s67.
[13] P. Holubar, M. Jilek, M. Sima, Present and possible future applications of superhard nanocomposite coatings, Surface and Coating Technology 133 (2000) 145–151.
[14] J.H. Yun, S.J. Heo, K.R. Kim, K.H. Kim, Synthesis and mechanical properties of $CrMoC_xN_{1-x}$ coatings deposited by a hybrid coating system, Journal of Vacuum Science and Technology A 26 (2008) 146–150.
[15] H. Ollendorf, D. Schneider, A comparative study of adhesion test methods for hard coatings, Surface and Coating Technology 113 (1999) 86–102.
[16] N. Kuratani, Y. Murakami, O. Imai, K. Ogata, Influences of intermediate Si–Ni thin film conditions on adhesion of Ni–TiN gradient thick films, Materials Chemistry and Physics 54 (1998) 313–316.
[17] E. Harry, A. Rouzaud, P. Juliet, Y. Pauleau, Adhesion and failure mechanisms of tungsten–carbon containing multilayered and graded coatings subjected to scratch tests, Thin Solid Films 342 (1999) 207.
[18] N.J.M. Carvalho, J.Th.M. DeHosson, Microstructure investigation of magnetron sputtered WC/C coatings deposited on steel substrates, Thin Solid Films 388 (2001) 150–159.
[19] J. Esteve, G. Zambrano, C. Rincón, E. Martinez, H. Galindo, P. Prieto, Mechanical and tribological properties of tungsten carbide sputtered coatings, Thin Solid Films 373 (2000) 282–286.
[20] Y.-C. Zhu, K. Yukimura, C.-X. Ding, P.-Y. Zhang, Tribological properties of nanostructured and conventional WC–Co coatings deposited by plasma spraying, Thin Solid Films 388 (2001) 277.
[21] R. Ospina, E. Restrepo-Parra, Y.C. Arango, H. Castillo, A. Devia, Study of W/WC coatings varying the substrate temperature, AIP Conference Proceedings 875 (2006) 240–244.
[22] A. Kumar, K. Singh, O.P. Pandey, Sintering behavior of nanostructured WC–Co composite, Ceramics International 37 (2011) 1415–1422.
[23] B.Q. Yang, X.P. Wang, H.X. Zhang, Z.B. Wang, P.X. Feng, Effect of substrate temperature variation on nanostructured WC films prepared using HFCVD technique, Materials Letters 62 (2008) 1547–1550.
[24] R. Ospina, H.A. Castillo, V. Benavides, E. Restrepo-Parra, Y.C. Arango, D.F. Arias, A. Devia, Influence of the annealing temperature on a crystal phase of W/WC bilayers grown by pulsed arc discharge, Vacuum 81 (2006) 373–377.
[25] V.J. Benavides, C.D. Salazar, M.E. Espitia, D.M. Devia, A. Devia, Study of TiC/a-C thin films growth by cathodic arc discharge varying the substrate temperature, Physica Scripta 131 (2008) 1–7.
[26] J.E. Sundgren, Structure and properties of TiN coatings, Thin Solid Films 128 (1985) 21–44.
[27] Y.H. Cheng, B.K. Tay, S.P. Lau, Influence of deposition temperature on the structure and internal stress of TiN films deposited by filtered cathodic vacuum arc, Journal of Vacuum Science and Technology A 20 (2002) 1270–1274.
[28] O.R. Monteiro, Thin film synthesis by energetic condensation, Annual Review of Materials Research 31 (2001) 111–137.
[29] H. Jiménez, E. Restrepo-Parra, A. Devia, Effect of the substrate temperature in ZrN coatings grown by the pulsed arc technique studied by XRD, Surface and Coatings Technology 201 (2006) 1594–1601.
[30] M. Larsson, M. Bromark, P. Hedenqvist, S. Hogmark, Deposition and mechanical properties of multilayered PVD Ti–TiN coatings, Surface and Coatings Technology 76–77 (1995) 202–205.
[31] J. Bruneaux, H. Cachet, M. Froment, A. Messad, Correlation between structural and electrical properties of sprayed tin oxide films with and without fluorine doping, Thin Solid Films 197 (1991) 129–142.
[32] U.C. Oh, J.H. Je, Effects of strain energy on the preferred orientation of TiN thin films, Journal of Applied Physics 74 (1993) 1692–1696.
[33] U.C. Oh, J.H. Je, J.Y. Lee, Change of the critical thickness in the preferred orientation of TiN films, Journal of Materials Research 10 (1995) 634–639.
[34] H. Oettel, R. Wiedemann, Residual stresses in PVD hard coatings, Surface and Coatings Technology 76–77 (1995) 265–273.
[35] V. Teixeira, Mechanical integrity in PVD coatings due to the presence of residual stresses, Thin Solid Films 392 (2001) 276–281.
[36] H. Oettel, R. Wiedemann, S. Preibler, Residual stresses in nitride hard coatings prepared by magnetron sputtering and arc evaporation, Surface and Coatings Technology 74–75 (1995) 273.
[37] G.B. Thompson, R. Banerjee, X.D. Zhang, P.M. Anderson, H.L. Fraser, Chemical ordering and texture in Ni–25 at% Al thin films, Acta Materialia 50 (2002) 643–651.
[38] H. Romanus, V. Cimalla, J.A. Schaefer, L. Spieb, G. Ecke, J. Pezoldt, Preparation of single phase tungsten carbide by annealing of sputtered tungsten–carbon layers, Thin Solid Films 359 (2000) 146–149.
[39] Y.Sh. Kim, Thermal treatment effects on the material and gas-sensing properties of room-temperature tungsten oxide nanorod sensors, Sensors and Actuators B 137 (2009) 297–304.
[40] J.-H. Wu, D.A. Rigneya, M.L. Falk, J.H. Sanders, A.A. Voevodin, J.S. Zabinski, Tribological behavior of WC/DLC/WS_2 nanocomposite coatings, Surface and Coatings Technology 188–189 (2004) 605–611.
[41] N. Radic, B. Pivac, F. Meinardi, Th. Koch, Raman study of carbon clusters in W–C thin films, Materials Science and Engineering A 396 (2005) 290–295.
[42] B.Q. Yang, X.P. Wang, H.X. Zhang, Z.B. Wang, P.X. Feng, Effect of substrate temperature variation on nanostructured WC films prepared using HFCVD technique, Materials Letters 62 (2008) 1547–1550.
[43] K. Nonaka, A. Takase, K. Miyakawa, Raman spectra of sol–gel-derived tungsten oxides, Journal of Materials Science Letters 12 (1993) 274–277.
[44] Z. Lu, S.M. Kanan, C.P. Tripp, Synthesis of high surface area monoclinic WO_3 particles using organic ligands and emulsion based methods, Journal of Materials Chemistry 12 (2002) 983–989.
[45] K. Hauffe, Oxidation of Metals, Plenum Press, New York, 1965.
[46] M. Gubisch, Y. Liu, L. Spiess, H. Romanus, S. Krischok, G. Ecke, Nanoscale multilayer WC/C coatings developed for nanopositioning: Part I. Microstructures and mechanical properties, Thin Solid Films 488 (2005) 132–139.
[47] Y. Pauleau, Ph. Gouy-Pailler, S. Paidassi, Structure and mechanical properties of hard W–C coatings deposited by reactive magnetron sputtering, Surface and Coatings Technology 54 (55) (1992) 324–328.
[48] A.A. Voevodin, J.P. O'Neill, S.V. Prasad, J.S. Zabinski, Nanocrystalline WC and WC/a-C composite coatings produced from intersected plasma fluxes at low deposition temperatures, Journal of Vacuum Scienc and Technology A: Vacuum Surface Films 17 (1999) 986–992.
[49] A. Czyzniewski, Deposition and some properties of nanocrystalline WC and nanocomposite WC/a-C:H coatings, Thin Solid Films 433 (2003) 180–185.
[50] J.-H. Huang, F.-Y. Ouyang, G.-P. Yu, Effect of film thickness and Ti interlayer on the structure and properties of nanocrystalline TiN thin films on AISI D_2 steel, Surface and Coatings Technology 201 (2007) 7043–7053.
[51] J. Gerth, U. Wiklund, The influence of metallic interlayers on the adhesion of PVD TiN coatings on high-speed steel, Wear 264 (2008) 885–892.
[52] K.-R. Lee, K.Y. Eun, I. Kim, J. Kim, Design of W buffer layer for adhesion improvement of DLC films on tool steels, Thin Solid Films 377–378 (2000) 261–268.
[53] S.B. Ogale, P. Karve, A.A. Kulkarni, R.P. Sharma, J.P. Prabjyyot, S.M. Karnetkar, Substrate and barrier layer considerations in the growth and properties of diamond and diamond-like carbon, Surface and Coatings Technology 76–77 (1995) 803–808.

[54] J.P. Celis, D. Drees, M.Z. Huq, P.Q. Wu, M. De Bonte, Hybrid processes—a versatile technique to match process requirements and coating needs, Surface and Coatings Technology 113 (1999) 165–181.
[55] C.R. Lin, C.T. Kuo, R.M. Chang, Application of heat treatment and dispersive strengthening concept in interlayer deposition to enhance diamond film adherence, Thin Solid Films 308–309 (1997) 273–278.
[56] H.P. Lorenz, Investigation of TiN as an interlayer for diamond deposition on steel, Diamond and Related Materials 4 (1995) 1088–1092.
[57] C.M. Fernandes, A.M.R. Senos, Cemented carbide phase diagrams: a review, International Journal of Refractory Metals and Hard Materials 29 (2011) 405–418.
[58] B. Vamsi Krishna, V.N. Misra, P.S. Mukherjee, P. Sharma, Microstructure and properties of flame sprayed tungsten carbide coatings, International Journal of Refractory Metals and Hard Materials 20 (2002) 355.
[59] P.J. Martin, R.L. Boxman, P.J. Martin, D.M. Sanders (Eds.), Noyes, Park Ridge, NJ, 1995.
[60] Q. Meng, N. Zhou, Y. Rong, S. Chen, T.Y. Hsu, Size effect on the Fe nanocrystalline phase transformation, Acta Materialia 50 (2002) 4563–4570.
[61] X.L. Peng, Z.H. Barber, T.W. Clyne, Surface roughness of diamond-like carbon films prepared using various techniques, Surface and Coatings Technology 138 (2001) 23.
[62] M. Devika, N. Koteeswara Reddy, K. Ramesh, V. Ganesan, E.S.R. Gopal, K.T. Ramakrishna, Influence of substrate temperature on surface structure and electrical resistivity of the evaporated tin sulphide films, Applied Surface Science 253 (2006) 1673–1676.